https://doi.org/10.5194/egusphere-2025-1231
Preprint. Discussion started: 28 April 2025

Seismic anisotropy under Zagros foreland from SKS splitting observations

Khalil Motaghi[1], Ayoub Kaviani[2], Wathiq Abdulnaby[3], Hanan Mahdi[4], Haydar Al-Shukri[4]

[1]Department of Earth Sciences, Institute for Advanced Studies in Basic Sciences (IASBS), Zanjan 45137-66731, Iran

[2]Institute of Geosciences, Goethe University, Frankfurt, Germany

[3]Seismological Laboratory of University of Basrah (SLUB), Department of Geology, College of Science, University of Basrah, Basrah, Iraq

[4]University of Arkansas at Little Rock (UALR), Little Rock, Arkansas, US

Correspondence: Khalil Motaghi (khalil1024@yahoo.com)

Abstract

We present SK[K]S splitting measurements from 18 newly deployed seismic stations in the foreland of the Zagros collision zone, providing new insights into asthenospheric flow and lithospheric deformation associated with the Arabian-Eurasian continental collision. Our results reveal two distinct fast-axis orientations: NE-SW in northern Iraq and NW-SE in the Mesopotamian Plain and Persian Gulf. The NE-SW anisotropy in northern Iraq aligns with fast-axis orientations observed in the Iranian-Anatolian Plateau and the azimuth of absolute plate motion, indicating large-scale asthenospheric flow as the primary influence across the northern Middle East. In contrast, the NW-SE anisotropy in the Mesopotamian Plain and Persian Gulf, characterized by smaller splitting times, parallels previously reported Pn anisotropy, suggesting a contribution from lithospheric mantle anisotropy, likely a remnant of past rifting. The influence of asthenospheric flow on the observed seismic anisotropy in this region appears minor. These findings refine our understanding of mantle dynamics and lithosphere-asthenosphere interactions in the Zagros collision zone.

Keywords: Anisotropy, Zagros collision, Mesopotamia, Asthenospheric flow, SK[K]S

https://doi.org/10.5194/egusphere-2025-1231
Preprint. Discussion started: 28 April 2025

1. Introduction

Seismic anisotropy is an important tool for investigating the dynamics of the Earth's mantle and the processes driving plate tectonics (e.g., Park and Levin, 2002; Long and Becker, 2010). It provides insights into deformation within the crust and upper mantle, and helps detect large-scale deep features such as mantle flows that are not easily identified by other geophysical methods (Silver and Chan, 1991). In this study, we focus on the foreland region of the Zagros continental collision zone, aiming to develop a geodynamic model that elucidates the interaction between mantle flow and continental lithosphere. Specifically, we investigate mantle anisotropy to characterize the interplay between the globally northeast-directed asthenospheric flow and the lithospheric root beneath the Zagros orogeny (Priestley et al., 2012). The dynamics of the lithospheric mantle in this region are shaped by shear and normal tractions associated with large-scale plate motions and localized mantle processes (Sandvol et al., 2003). This research represents the first investigation of mantle anisotropy within the foreland basin of the Arabia-Eurasia plate boundary, encompassing eastern Iraq and the Persian Gulf (Fig. 1).

Seismic anisotropy in the mantle lithosphere, asthenosphere, or both, can yield teleseismic shear-wave splitting (Silver and Chan, 1991; Silver and Holt, 2002). In the Middle East, anisotropy studies based on splitting analysis of core-refracted phases (SKS and SKKS) have revealed a consistent NE-oriented asthenospheric flow beneath the Anatolian plate and northern Iran, corresponding to the global mantle flow in the no-net rotation (NNR) reference frame (Kaviani et al., 2021; Paul et al., 2014; Arvin et al., 2021). Near the southwestern edge of the Arabian plate, this flow is deflected northward by the Afar plume (Hansen et al., 2006). However, the Zagros collision zone in western Iran exhibits a more intricate anisotropy pattern,

https://doi.org/10.5194/egusphere-2025-1231
Preprint. Discussion started: 28 April 2025

influenced by deformation of the thick Arabian lithosphere (Priestley et al., 2012; Sadegh-Bagherabadi et al., 2018b) and deflected asthenospheric flow in response to significant variations in lithospheric thickness compared to adjacent regions (Kaviani et al., 2021). Despite the significance of anisotropic features in this area, the Zagros foreland remains underexplored due to logistical challenges. The partial coverage of the region by the Persian Gulf complicates seismic data acquisition (Fig. 1), and eastern Iraq has historically lacked adequate seismic monitoring. To address this knowledge gap, this study uses new seismic data from a regional network of 17 stations in Iraq and a newly established station in the Persian Gulf. The Iraqi stations, established as part of a network enhancement initiative by the Lawrence Livermore National Laboratory (LLNL) of the U.S. Department of Energy, provide observations from a previously under-sampled region. Using shear wave splitting analysis of SKS and SKKS phases, we investigate the interaction between the asthenospheric flow beneath the Arabian plate and the thick lithospheric root at its northern edge, focusing on the Zagros foreland region.

This study addresses two primary scenarios for interaction between the asthenospheric flow and the lithosphere root beneath the Zagros foreland. First, the thick lithospheric root may force the asthenospheric channel to greater depths, allowing the asthenospheric flow to continue northwestward in alignment with the NNR frame motion. Alternatively, the lithosphere root may act as a barrier, redirecting the asthenospheric flow toward shallower regions beneath adjacent thinner lithosphere, such as northwest Iran, the Anatolian plate, or the oceanic plate of the Makran subduction zone. In addition to asthenospheric flow, we also consider the possibility of "frozen" anisotropy, inherited from the study region's tectonic history as part of the northern Gondwana landmass.

2. Data and method

https://doi.org/10.5194/egusphere-2025-1231
Preprint. Discussion started: 28 April 2025

A new regional seismic network was installed in Iraq (Fig. 1) through a collaboration with the University of Arkansas at Little Rock (UALR). Data acquisition began in 2014 through a multi-institutional collaboration (Abdulnaby et al., 2020). Table 1 provides the station coordinates and the time intervals during which data were accessible. Most stations were repositioned over time, with data collection periods ranging from five months to nine years (Table 1). To enhance lateral coverage in the Zagros foreland, we also incorporated data from a newly established seismic station situated on Khark Island in the Persian Gulf. This station is operated by the International Institute of Earthquake Engineering and Seismology in Iran.

We extracted three-component waveforms from teleseismic earthquakes with magnitudes ≥ 6.0 from epicentral distances between 90° and 140°. A total of 3256 records met these criteria. Two splitting parameters—Φ (fast-axis anisotropy orientation) and δt (splitting time between fast and slow polarizations)—were estimated using the rotation-correlation method of Bowman and Ando (1987). Before performing the splitting analysis, we visually examined the waveforms to confirm low noise levels and to ensure that the SK[K]S phases were not distorted by other teleseismic phases with similar arrival times. Band-pass filtering was applied using visually selected cutoff periods, with low cutoff periods ranging from 5 to 10 s and high cutoff periods ranging from 20 to 30 s.

We manually selected the analysis window around the theoretical SK[K]S onset, calculated using the IASP91 standard velocity model (Kennett and Engdahl, 1991). The window length was chosen to include at least one period of the clearly observable target phases. Final splitting parameters were retained in the dataset after meeting the following quality criteria: (1) a signal-to-noise ratio > 2 for the radial component within the analysis window, (2) a minimum correlation coefficient > 0.90 between the fast and slow components, (3) elliptical particle motion before correcting for anisotropy and nearly linear particle motion after correction, (4) a measured splitting time exceeding 0.5 s, and (5) at least a 50% reduction in energy on the transverse component after anisotropy correction using the calculated splitting parameters, in cases of non-null measurements. Measurements showing initial linear particle motion were classified as null, indicating no splitting.

Figure 2 presents two examples of the splitting analysis, illustrating the energy on the original transverse (Sh) component and the elliptical particle motion of the horizontal components, both indicative of shear wave splitting. Main criteria for reliable measurements include the observation of linear particle motion and significant energy reduction on the Sh component following correction using the estimated splitting parameters. The final dataset includes 155 reliable non-null measurements and 630 null measurements, as shown in Figures 3 and 4.

3. Results

Figure 3 shows the rose diagrams of both null and non-null measurements for 18 new stations in the Zagros foreland. Figure 4 presents the rose diagrams for non-null splitting measurements at seismic station locations, with individual measurements (represented by red bars) projected to their piercing points, alongside measurements from previous studies at a depth of 200 km. At stations AMR1, AMR2, BSR2, NSR1, NSR3, NSR4, ANB1, and KIR1, the non-null measurements exhibit a consistent unimodal pattern (Fig. 3). To explore the origin of the bimodal fast-axis orientations, individual non-null measurements projected to their piercing points provide valuable insights (Figure 4b). The results reveal distinct fast-axis orientations east and west of station SLY1, as well as north and south of station DHK1, both situated near the edge of the Zagros orogeny. These spatial variations suggest that the observed bimodal pattern of fast-axis orientations primarily results from lateral rather than vertical heterogeneities in the anisotropic structure.

https://doi.org/10.5194/egusphere-2025-1231
Preprint. Discussion started: 28 April 2025

The fast axis orientations across the study region can be categorized into two main patterns. First, in southern Iraq and the Persian Gulf (latitude < 32°N), the orientations are predominantly NW-SE, sub-parallel to the Zagros orogeny and perpendicular to the absolute plate motion (APM) direction within the no-net-rotation (NNR) reference frame (Kreemer et al., 2014; Fig. 1). This pattern is observed at stations BSR1, BSR2, NSR1, NSR2, NSR4, AMR1, AMR2, SAM2, and KUT1 and extends into the Persian Gulf at station KHRK, marking the offshore continuation of the Zagros foreland basin. Second, in northern Iraq (latitude > 33°N), the fast axis orientations are primarily NE-SW, perpendicular to the Zagros orogeny and sub-parallel to the APM vector, as observed at stations ANB1, ANB2, KIR1, SLY1, and DHK1. Station KAR2, located near the boundary between these two regions, shows almost null SK(K)S splitting, with 94 null measurements and 1 non-null measurements from a northeast back-azimuth (Fig. 3 and Table 1). This suggests the presence of two dominant anisotropic features with perpendicular orientations in the northern and southern sections of the study region. The average splitting time is 0.82 s, which is lower than the values reported in surrounding regions, including the Inner Arabian Platform, Anatolian Plate, and the Zagros collision zone, where splitting times exceed 1 s (Paul et al., 2014; Qaysi et al., 2018; Kaviani et al., 2021), as shown in Figure 5.

4. Comparison with previous studies

To investigate patterns of upper mantle seismic anisotropy, we combined our dataset with all available SK[K]S measurements from the Middle East. This merging allows us to assess how the results of this study align with or diverge from previous observations. Figure 6 presents maps comparing our measurements with those from earlier studies in neighboring regions, including the Iranian Plateau and eastern Anatolian Plateau (Kaviani et al., 2021), northwestern

https://doi.org/10.5194/egusphere-2025-1231
Preprint. Discussion started: 28 April 2025

Iran (Arvin et al., 2021), the northern Zagros (Sadeghi-Bagherabadi et al., 2018a, 2018b), and the Inner Arabian Platform (Qaysi et al., 2018). In the left panels of Figure 6, individual SK[K]S measurements are displayed, with red bars representing the new measurements and blue bars indicating those from previous studies. Each measurement is projected onto its ray-piercing point at depths of 100 km, 200 km, and 300 km, shown in panels a, c, and e, respectively, to account for uncertainty in the depth of anisotropy.

Our results show a high degree of consistency with previous measurements, particularly in southern Iraq and the Persian Gulf, where NW-SE-oriented fast axes are observed. Similarly, in northern Iraq, the NE-SW-oriented fast axes align well with prior measurements in northern Iraq and eastern Turkey (Kaviani et al., 2021). This agreement affirms that our findings extend the observation of upper mantle anisotropy across the Zagros collision zone and enhance understanding of mantle flow and deformation beneath this tectonically active region.

To further visualize the azimuthal anisotropy patterns, we calculated vector averages of the individual splitting parameters projected at respective depths and within the Fresnel zone of SK[K]S waves, utilizing sensitivity kernels as calculated by Monteiller and Chevrot (2011). The interpolated anisotropy fields, shown in the right panels of Figure 6, demonstrate that the anisotropic patterns remain largely consistent across different depth levels. This consistency suggests a relatively simple and coherent anisotropic structure beneath the study region.

5. Discussion

5.1 A uniform asthenospheric flow in the northern Middle East

The anisotropy measurements in Figure 4 consistently show a fast axis orientation toward the NE-SW in northern Iraq which is consistent with the NE-SW orientations in the Anatolian

Plateau and northwestern Iran (Fig. 6). This alignment closely correlates with the azimuth of the APM direction in the NNR frame (Kreemer et al., 2014). The strong correlation across such a vast region suggests the dominance of a large-scale viscous flow in the asthenosphere as the prevailing mechanism beneath the northern Middle East (Sandvol et al., 2003; Paul et al., 2014).

The dominance of asthenospheric flow is consistent with the presence of a relatively thin lithosphere beneath the northern Middle East (Priestley and McKenzie, 2013), as illustrated in Figure 7d. This correlation is significant because it indicates that the lithosphere has a minor influence on the accumulated anisotropy responsible for the observed SK[K]S splitting. Further evidence supporting this interpretation comes from S-receiver function analyses in northwestern Iran and eastern Turkey, which reveal a thin lithosphere (ranging from 80 to 100 km in thickness) beneath eastern Anatolia, the Bitlis suture zone (e.g., Kind et al., 2015), northwestern Iran (e.g., Taghizadeh-Farahmand et al., 2010), and northeastern Iran (e.g., Taghizadeh-Farahmand et al., 2013). Notably, the lithospheric mantle is entirely absent beneath portions of the Anatolian Plate (Gök et al., 2007).

Furthermore, the alignment of the APM with the orientation of SK[K]S measurements (i.e., orientation of asthenospheric flow) suggests strong coupling between the thin lithosphere and the underlying mantle in the northern Middle East. This observation reinforces the conclusion that asthenospheric flow is the primary driver of plate tectonics in this region.

A comparison of the azimuthal anisotropy of Pn waves (Lü et al., 2017) with the fast-axis orientations of SK[K]S waves projected to a depth of 75 km reveals different anisotropic patterns across northern Iraq (Fig. 7c). This discrepancy suggests the presence of vertical anisotropic layering, where distinct sources of anisotropy influence Pn and SK[K]S waves. We propose that anisotropy within the lithospheric mantle has a limited influence on SK[K]S

https://doi.org/10.5194/egusphere-2025-1231
Preprint. Discussion started: 28 April 2025

splitting due to the thin lithospheric mantle in this region, while SK[K]S splitting primarily reflects sub-lithospheric anisotropy associated with asthenospheric flow.

It is noteworthy that the tectonics of northern Iraq and eastern Turkey are dominated by the active convergence between the Arabian Plate and Eurasia, accommodated by the westward escape of Anatolia (Dewey et al., 1986; McClusky et al., 2000). Despite the complexity of this tectonic junction, our azimuthal anisotropic patterns, as illustrated in Figures 4, 6, and 7, remain relatively unaffected. This suggests that post-collisional tectonics in the region did not produce a coherent or simple anisotropic texture in the lithosphere.

5.2 Patterns of anisotropy beneath the Zagros Foredeep

In southern Iraq and the Persian Gulf, the observed anisotropic fast-axis directions exhibit a NW-SE orientation, perpendicular to the absolute plate motion and subparallel to the trend of the Zagros orogeny. Observing these anisotropy orientations just behind a lithospheric root beneath the Zagros orogeny (Fig. 7d) supports the concept of circular mantle flow around the Zagros keel, as proposed by Kaviani et al. (2021). Their analysis of SK[K]S measurements in the Iranian Plateau, covering the northern and eastern flanks of the Zagros orogeny, revealed anisotropic axes encircling the Zagros lithospheric keel. This behavior, in which the lithosphere acts as a barrier to horizontal asthenospheric flow when it is considerably thicker than the surrounding regions, has been observed beneath the South American cratonic keel (Miller and Becker, 2012) and eastern North America (Fouch et al., 2000).

At first glance, new data from the Zagros foreland in southern Iraq and the Persian Gulf appear consistent with this model. However, a comparison of SK[K]S and Pn anisotropy in the same region (Fig. 7c) reveals parallel orientations, indicating that at least part of the observed

https://doi.org/10.5194/egusphere-2025-1231
Preprint. Discussion started: 28 April 2025

anisotropy originates in the lithospheric mantle. Additionally, the splitting time beneath the Mesopotamian Plain is significantly smaller than in surrounding regions, such as eastern Anatolia and the Inner Arabian Platform (Fig. 5), where anisotropy is primarily driven by asthenospheric flow (Hansen et al., 2006; Paul et al., 2014; Qaysi et al., 2018; Kaviani et al., 2021). This suggests that while asthenospheric flow beneath the Mesopotamian Plain may still generate anisotropy, its influence is significantly weaker than in nearby regions. This reduction is likely due to the presence of a more complex asthenospheric flow near the lithospheric keel beneath the Zagros orogeny (Fig. 7d). The lithospheric root causes substantial variations in lithospheric thickness in adjacent areas, leading the asthenospheric flow dipping and being deflected beneath the Mesopotamian Plain and the Zagros orogeny, as suggested by Sadeghi-Bagherabadi et al. (2018b).

The dipping of asthenospheric flow can reduce the generation of azimuthal anisotropy, thereby minimizing its contribution to the observed SK[K]S splitting in this region. In this scenario, the small splitting times (Fig. 5) are partly attributed to the presence of a ~150 km thick lithosphere beneath the region (Fig. 7d), with asthenospheric flow playing a limited role. An alternative explanation is that the fast axis orientation from SK[K]S waves is parallel to the slow axis within the lithospheric mantle, resulting in reduced splitting times recorded by SK[K]S phases. Although our measurements do not reveal a clear pattern of asthenospheric flow behind the lithospheric root beneath the Mesopotamian Plain, the absence of strong asthenospheric flow in the observed splitting time offers insights into the regional flow dynamics. Rather than rotating around the lithospheric root, asthenospheric flow may instead migrate beneath it at greater depths. While this interpretation is not definitive, the lack of significant splitting immediately behind the lithospheric root represents a novel observation that challenges the concept of circular asthenospheric flow, suggesting a more complex flow pattern.

https://doi.org/10.5194/egusphere-2025-1231
Preprint. Discussion started: 28 April 2025

5.3 Origin of Anisotropy in the Zagros Foreland Lithospheric Mantle

The NW-SE fast-axis orientation within the lithospheric mantle beneath the Mesopotamian Plain and Persian Gulf raises questions about its origin. One possibility for the existence of such anisotropy is that it results from pure shear deformation within the lithosphere due to the continental collision in the Zagros orogeny. However, this scenario is unlikely because the Arabian lithosphere is cold and strong, with temperatures below 900°C beneath the Moho boundary (Priestley et al., 2012). Such low temperatures inhibit olivine mobility, preventing alignment with the maximum strain direction (Nicolas and Christensen, 1987). An alternative explanation is that the lithospheric mantle anisotropy reflects a "frozen" signature from earlier tectonic events. Several significant tectonic episodes have shaped the region, including the Precambrian Amar Collision (~640–620 Ma; Al-Husseini, 2000), the NAJD Rift System (~570–530 Ma; Husseini, 1988, 1989; Husseini and Husseini, 1990), the Neotethys rifting during the Triassic and Late Jurassic (e.g., Fadhel and Al-Rahim, 2019), and the ongoing Zagros continental collision (~35 Ma to present; Jackson and McKenzie, 1984; Alavi, 2004).

The consistency of the NW-SE fast-axis orientation with the Zagros orogeny, its alignment with the suture boundary between the Arabian and Eurasian plates, and its confinement to the Zagros foreland depression (Fig. 4) suggest a connection to Neotethys rifting. Rift systems elevate lithospheric temperatures, generating rift-parallel anisotropy aligned with the rift axis. The Mesozoic rift axis between the Arabian and Eurasian plates was along the suture boundary between the two plates. However, if diffuse rifting occurred between them, remnants of this rift may also be preserved in structures parallel to the main axis.

Evidence for diffuse rifting in the region comes from previous geological and seismological studies (Abdulnaby et al., 2020). Abdulnaby et al. (2020) analyzed the P receiver functions

https://doi.org/10.5194/egusphere-2025-1231
Preprint. Discussion started: 28 April 2025

beneath stations used in this study and found a crustal root beneath the southeastern Mesopotamian Plain as thick as those in the Zagros collision zone. They proposed that the lack of isostatic balance between the large crustal thickness and low topography in the region results from successive rifting events. These events caused vertical loading from the accumulation of thick sedimentary deposits in the basin, reaching thicknesses of up to 14 km over fault-bounded depocenters, leading to the formation of crustal roots (Abdulnaby et al., 2020). The Abu Jir-Euphrates fault is clearly observed as a basement fault step in seismic lines (Mohammed, 2006) and bounds the southwest margin of the rift system (e.g., Fadhel and Al-Rahim, 2019). This fault system, inherited from Triassic passive-margin extension, was reactivated during Middle to Late Jurassic rifting, forming graben-horst structures in the Mesopotamian Plain (Numan, 1997, 2000). Continuous subsidence along these faults since the Late Jurassic allowed thick sedimentary sequences to accumulate in this tectonic depression (Jassim and Göff, 2006).

In summary, our findings suggest that the uniform NW-SE fast-axis anisotropy within the lithosphere of the Mesopotamian Plain likely originates from successive Mesozoic rifting of the northeastern Arabian platform. This lithosphere has remained largely intact despite the relatively young Zagros collision. The southwestward migration of the Zagros deformation front (ZFF) overprinted the eastern boundary of the graben beneath the Mesopotamian Plain through thrust faulting and folding with opposing dips in the sedimentary cover. Abdulnaby et al. (2016a, 2016b) and Darweesh et al. (2017) proposed a southwestward dip of 60° for the eastern margin of the basin beneath the ZFF. Collectively, these findings confirm that the Mesopotamian Plain has remained largely unaffected by deformation from the Zagros collision zone. Consequently, older tectonic events, such as Mesozoic rifting, are the most likely source of the preserved lithospheric mantle anisotropy. This study provides the first evidence of such rifting effects recorded in the lithospheric mantle.

https://doi.org/10.5194/egusphere-2025-1231
Preprint. Discussion started: 28 April 2025

6. Conclusions

This study presents SK[K]S splitting measurements from 18 newly deployed seismic stations in the foreland of the Zagros collision zone, filling a gap in the anisotropy map of the Middle East. Our dataset of 155 non-null measurements reveals two distinct fast-axis orientations: a NE-SW trend in northern Iraq and a NW-SE trend in the Mesopotamian Plain and Persian Gulf.

By integrating our results with recent anisotropy data from the Iranian-Anatolian Plateau, we identify a consistent NE-SW fast-axis orientation across the northern Middle East, including northern Iraq. This orientation closely aligns with the azimuth of absolute plate motion in the no-net-rotation reference frame, indicating that large-scale asthenospheric flow governs the observed anisotropy. The agreement between the absolute plate motion and asthenospheric flow suggests strong lithosphere-asthenosphere coupling, supporting the interpretation that asthenospheric flow is a key driver of plate dynamics in this region.

In contrast, the NW-SE anisotropy in the Mesopotamian Plain and Persian Gulf is associated with smaller splitting times, paralleling previously reported Pn anisotropy and suggesting a contribution from the lithospheric mantle. This finding challenges prior models of asthenospheric flow encircling the Zagros lithospheric keel, which implied weak lithosphere-asthenosphere coupling. Instead, the weak anisotropy beneath the Mesopotamian Plain may reflect steeply dipping asthenospheric flow beneath a laterally variable lithospheric thickness, resulting in reduced azimuthal anisotropy at the surface.

The NW-SE-orientated lithospheric anisotropy aligns with the suture boundary between the Arabian Plate and Eurasia and may represent a relic of diffuse Mesozoic rifting responsible for the formation of the Mesopotamian depression. These findings underscore the dual influence of asthenospheric flow and lithospheric deformation on seismic anisotropy in the Zagros

https://doi.org/10.5194/egusphere-2025-1231
Preprint. Discussion started: 28 April 2025

collision zone, offering new insights into mantle dynamics and lithosphere-asthenosphere interactions in continental collision settings.

Acknowledgements

We are grateful to the Lawrence Livermore National Laboratory (LLNL) for supporting the installation of broadband seismic stations in Iraq. We also like to thank the University of Arkansas, Little Rock, for partially supporting this research.

Data availability

Continuous data from 17 Iraqi stations used in this study are available through the Incorporated Research Institutions for Seismology (IRIS).

Author contribution

KM analyzed the data, prepared figures, interpreted the results, and wrote the initial draft of the manuscript. AK developed the code, supervised the data analysis, prepared figures, and revised the manuscript. WA conducted the field survey, collected raw data, provided the data, and revised the manuscript. HM secured funding for data collection in Iraq and revised the manuscript. HA secured funding for data collection in Iraq and revised the manuscript.

Competing interests

None of the authors has any competing interests.

References

Abdulnaby, W., Al-Mohmed, R., & Mahdi, M. (2016). Seismicity and recent stress regime of Diyala City, Iraq–Iran border. Modeling Earth Systems and Environment, 2, 1-8.

https://doi.org/10.5194/egusphere-2025-1231
Preprint. Discussion started: 28 April 2025

Abdulnaby, W., Mahdi, M., Al-Mohmed, R., & Mahdi, H. H. (2016). Seismotectonic of Badra-Amarah Fault, Iraq-Iran border. IOSR Journal of Applied Geology and Geophysics (IOSR-JAGG), 4(3), 27-33.

Abdulnaby, W., Motaghi, K., Shabanian, E., Mahdi, H., Al-Shukri, H., & Gök, R. (2020). Crustal structure of the Mesopotamian Plain, east of Iraq. Tectonics, 39(11), e2020TC006225.

Alavi, M. (2004). Regional stratigraphy of the Zagros fold-thrust belt of Iran and its proforeland evolution. American journal of Science, 304(1), 1-20.

Al-Husseini, M. I. (2000). Origin of the Arabian Plate structures: Amar collision and Najd rift. GeoArabia, 5(4), 527-542.

Arvin, S., Sobouti, F., Priestley, K., Ghods, A., Motaghi, K., Tilmann, F., & Eken, T. (2021). Seismic anisotropy and mantle deformation in NW Iran inferred from splitting measurements of SK (K) S and direct S phases. Geophysical Journal International, 226(2), 1417-1431.

Bowman, J. R., & Ando, M. (1987). Shear-wave splitting in the upper-mantle wedge above the Tonga subduction zone. Geophysical Journal International, 88(1), 25-41.

Celli, N. L., Lebedev, S., Schaeffer, A. J., & Gaina, C. (2020). African cratonic lithosphere carved by mantle plumes. Nature communications, 11(1), 92.

Darweesh, H. A., Obed, A. Z. M., & Albadran, B. N. (2017). Structural study of basins configuration in Mesopotamian area. International journal of engineering and applied sciences, 4(9), 54-58.

Dewey, J. F., Hempton, M. R., Kidd, W. S. F., Saroglu, F. A. M. C., & Şengör, A. M. C. (1986). Shortening of continental lithosphere: the neotectonics of Eastern Anatolia—a young collision zone. Geological Society, London, Special Publications, 19(1), 1-36.

Fadhel, M. S., & Al-Rahim, A. M. (2019). A new tectono sedimentary framework of the Jurassic succession in the Merjan oil field, Central Iraq. Journal of Petroleum Exploration and Production Technology, 9(4), 2591-2603.

Fouad, S. F. (2010a). Tectonic evolution of the Mesopotamia Foredeep in Iraq. Iraqi Bulletin of Geology and Mining, 6(2), 41–53.

Fouad, S. F. (2010b). Tectonic map of Iraq, Scale 1: 1000 000 (3rd ed.). Baghdad, Iraq: Geological Survey and Mineral Investigation (GEOSURV).

Fouch, M. J., Fischer, K. M., Parmentier, E. M., Wysession, M. E., & Clarke, T. J. (2000). Shear wave splitting, continental keels, and patterns of mantle flow. Journal of Geophysical Research: Solid Earth, 105(B3), 6255-6275.

Gök, R., Pasyanos, M. E., & Zor, E. (2007). Lithospheric structure of the continent—continent collision zone: eastern Turkey. Geophysical Journal International, 169(3), 1079-1088.

Hansen, S., Schwartz, S., Al-Amri, A., & Rodgers, A. (2006). Combined plate motion and density-driven flow in the asthenosphere beneath Saudi Arabia: Evidence from shear-wave splitting and seismic anisotropy. Geology, 34(10), 869-872.

https://doi.org/10.5194/egusphere-2025-1231
Preprint. Discussion started: 28 April 2025

Husseini, M. I. (1988). The Arabian infracambrian extensional system. Tectonophysics, 148(1-2), 93-103.

Husseini, M. I. (1989). Tectonic and deposition model of late Precambrian-Cambrian Arabian and adjoining plates. AAPG Bulletin, 73(9), 1117-1131.

Husseini, M. I., & Husseini, S. I. (1990). Origin of the Infracambrian salt basins of the Middle East. Geological Society, London, Special Publications, 50(1), 279-292.

Jackson, J., & McKenzie, D. (1984). Active tectonics of the Alpine—Himalayan Belt between western Turkey and Pakistan. Geophysical Journal International, 77(1), 185-264.

Jassim, S. Z., & Göff, J. C. (2006). Geology of Iraq. Dolin, Prague and Moravian Museum, Brno, Czech Republic, p. 341.

Kaviani, A., Mahmoodabadi, M., Rümpker, G., Pilia, S., Tatar, M., Nilfouroushan, F., ... & Ali, M. Y. (2021). Mantle-flow diversion beneath the Iranian plateau induced by Zagros' lithospheric keel. Scientific reports, 11(1), 2848.

Kennett, B. L. N., & Engdahl, E. R. (1991). Traveltimes for global earthquake location and phase identification. Geophysical Journal International, 105(2), 429-465.

Kind, R., Eken, T., Tilmann, F., Sodoudi, F., Taymaz, T., Bulut, F., ... & Schneider, F. (2015). Thickness of the lithosphere beneath Turkey and surroundings from S-receiver functions. Solid Earth, 6(3), 971-984.

Kreemer, C., Blewitt, G. & Klein, E.C., (2014). A geodetic plate motion and Global Strain Rate Model, Geochem., Geophys., Geosyst., 15(10), 3849–3889.

Long, M. D., & Becker, T. W. (2010). Mantle dynamics and seismic anisotropy. Earth and Planetary Science Letters, 297(3-4), 341-354.

Lü, Y., Ni, S., Chen, L., & Chen, Q. F. (2017). Pn tomography with Moho depth correction from eastern Europe to western China. Journal of Geophysical Research: Solid Earth, 122(2), 1284-1301.

Mcclusky, S., Balassanian, S., Barka, A., Demir, C., Ergintav, S., Georgiev, I., ... & Veis, G. (2000). Global Positioning System constraints on plate kinematics and dynamics in the eastern Mediterranean and Caucasus. Journal of Geophysical Research: Solid Earth, 105(B3), 5695-5719.

Miller, M. S., & Becker, T. W. (2012). Mantle flow deflected by interactions between subducted slabs and cratonic keels. Nature Geoscience, 5(10), 726-730.

Mohammed, S. A. (2006). Megaseismic section across the northeastern slope of the Arabian Plate, Iraq. GeoArabia, 11(4), 77-90.

Monteiller, V., and S. Chevrot, 2011. High-resolution imaging of the deep anisotropic structure of the San Andreas Fault system beneath southern California, Geophys. J. Int., 186, 418-446

Nicolas, A., & Christensen, N. I. (1987). Formation of anisotropy in upper mantle peridotites-A review. Composition, structure and dynamics of the lithosphere-asthenosphere system, 16, 111-123.

NOAA National Centers for Environmental Information, (2022). ETOPO 2022 15 Arc-Second Global Relief Model. NOAA National Centers for Environmental Information.

Numan, N. M. S. (1997). A plate tectonic scenario for the phanerozoic succession in Iraq. Journal of the Geological Society of Iraq, 30(2), 85–110.

Numan, N. M. S. (2000). Major cretaceous tectonic events in Iraq. Rafidain Journal of Science, 11(3), 32–52.

Park, J., & Levin, V. (2002). Seismic anisotropy: tracing plate dynamics in the mantle. Science, 296(5567), 485-489.

Paul, A., Karabulut, H., Mutlu, A. K., & Salaün, G. (2014). A comprehensive and densely sampled map of shear-wave azimuthal anisotropy in the Aegean–Anatolia region. Earth and Planetary Science Letters, 389, 14-22.

Priestley, K., McKenzie, D., Barron, J., Tatar, M., & Debayle, E. (2012). The Zagros core: Deformation of the continental lithospheric mantle. Geochemistry, Geophysics, Geosystems, 13(11).

Priestley, K., & McKenzie, D. (2013). The relationship between shear wave velocity, temperature, attenuation and viscosity in the shallow part of the mantle. Earth and Planetary Science Letters, 381, 78-91.

Qaysi, S., Liu, K. H., & Gao, S. S. (2018). A database of shear-wave splitting measurements for the Arabian Plate. Seismological Research Letters, 89(6), 2294-2298.

Sadeghi-Bagherabadi, A., Sobouti, F., Ghods, A., Motaghi, K., Talebian, M., Chen, L., ... & He, Y. (2018a). Upper mantle anisotropy and deformation beneath the major thrust-and-fold belts of Zagros and Alborz and the Iranian Plateau. Geophysical Journal International, 214(3), 1913-1918.

Sadeghi-Bagherabadi, A., Margheriti, L., Aoudia, A., & Sobouti, F. (2018b). Seismic anisotropy and its geodynamic implications in Iran, the easternmost part of the Tethyan Belt. Tectonics, 37(12), 4377-4395.

Sandvol, E., Turkelli, N., Zor, E., Gök, R., Bekler, T., Gurbuz, C., ... & Barazangi, M. (2003). Shear wave splitting in a young continent-continent collision: An example from eastern Turkey. Geophysical Research Letters, 30(24).

Silver, P. G., & Chan, W. W. (1991). Shear wave splitting and subcontinental mantle deformation. Journal of Geophysical Research: Solid Earth, 96(B10), 16429-16454.

Silver, P. G., & Holt, W. E. (2002). The mantle flow field beneath western North America. Science, 295(5557), 1054-1057.

Sissakian, V., Shihab, A. T., Al-Ansari, N., & Knutsson, S. (2017). New tectonic finding and its implications on locating Oilfields in parts of the Gulf region. Journal of Earth Sciences and Geotechnical Engineering, 7(3), 51-75.

Taghizadeh-Farahmand, F., Sodoudi, F., Afsari, N., & Ghassemi, M. R. (2010). Lithospheric structure of NW Iran from P and S receiver functions. Journal of seismology, 14, 823-836.

https://doi.org/10.5194/egusphere-2025-1231
Preprint. Discussion started: 28 April 2025

Taghizadeh-Farahmand, F., Sodoudi, F., Afsari, N., & Mohammadi, N. (2013). A detailed receiver function image of the lithosphere beneath the Kopeh-Dagh (Northeast Iran). Journal of seismology, 17, 1207-1221.

Figure 1

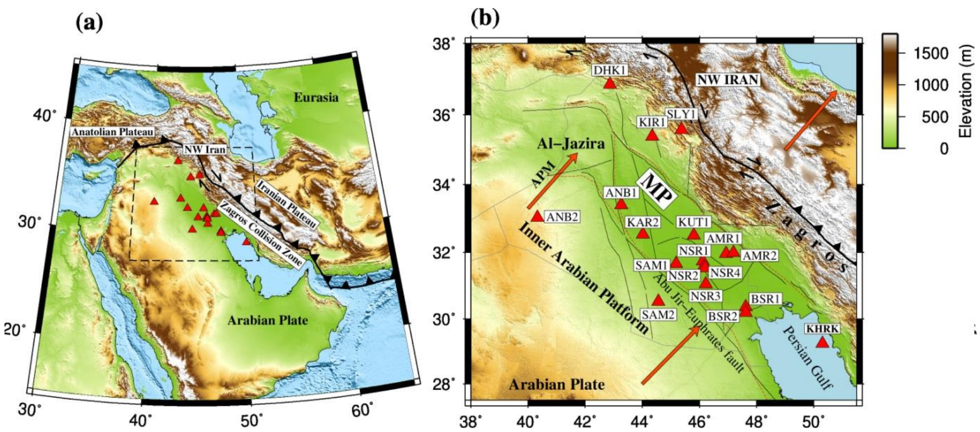

Figure 1: (a) Topographic Map of the Middle East. The triangles indicate the locations of 18 seismic stations within the study area. The solid lines mark the Bitlis-Zagros suture boundary. The dashed-line rectangle outlines the boundaries of the map displayed in panel (b). (b) Topographic Map of Mesopotamian Foredeep, situated in the foreland of the Zagros collision zone. The red dashed line indicates the tectonic division of Iraq as proposed by Fouad (2010a, 2010b) and Sissakian et al. (2017), separating the Inner Arabian Platform from the Outer Arabian Platform, which includes the Mesopotamian Foredeep. Al-Jazira, and Zagros collision zone. Arrows represent the absolute plate motion (APM) vectors from Kreemer et al. (2014). Thin black lines mark the location of basement faults within the Zagros Foreland Basin. Topographic and bathymetric data were obtained from the ETOPO1 global relief model (NOAA NCEI, 2022).

https://doi.org/10.5194/egusphere-2025-1231
Preprint. Discussion started: 28 April 2025

Figure 2

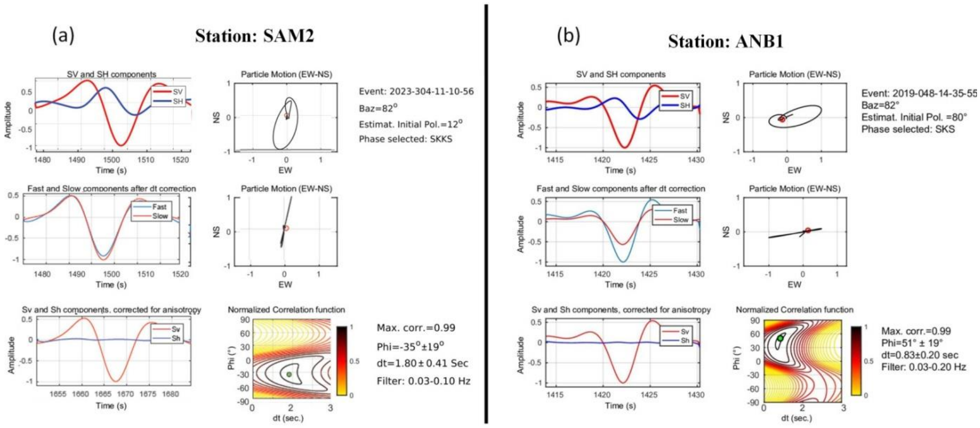

Figure 2: Examples of shear-wave splitting measurements using the rotation-correlation method. The locations of the two stations can be inferred from Figure 1b. (a) Single-event measurement at station SAM2. Data have been filtered to retain periods between 10 and 30 s. Information about the event is provided in the top right corner. The left panels, from top to bottom, display the original radial (red) and transverse (blue) seismograms, corrected fast (blue) and slow (red) components, and corrected radial (red) and transverse (blue) components, respectively. The right panels, from top to bottom, show the initial particle motion, the corrected particle motion, and the contour plot of the normalized correlation function with the optimal splitting parameter indicated by a green circle. The obtained splitting parameters are written in the bottom right corner. (b) Similar to (a) but for station ANB1.

https://doi.org/10.5194/egusphere-2025-1231
Preprint. Discussion started: 28 April 2025

Figure 3

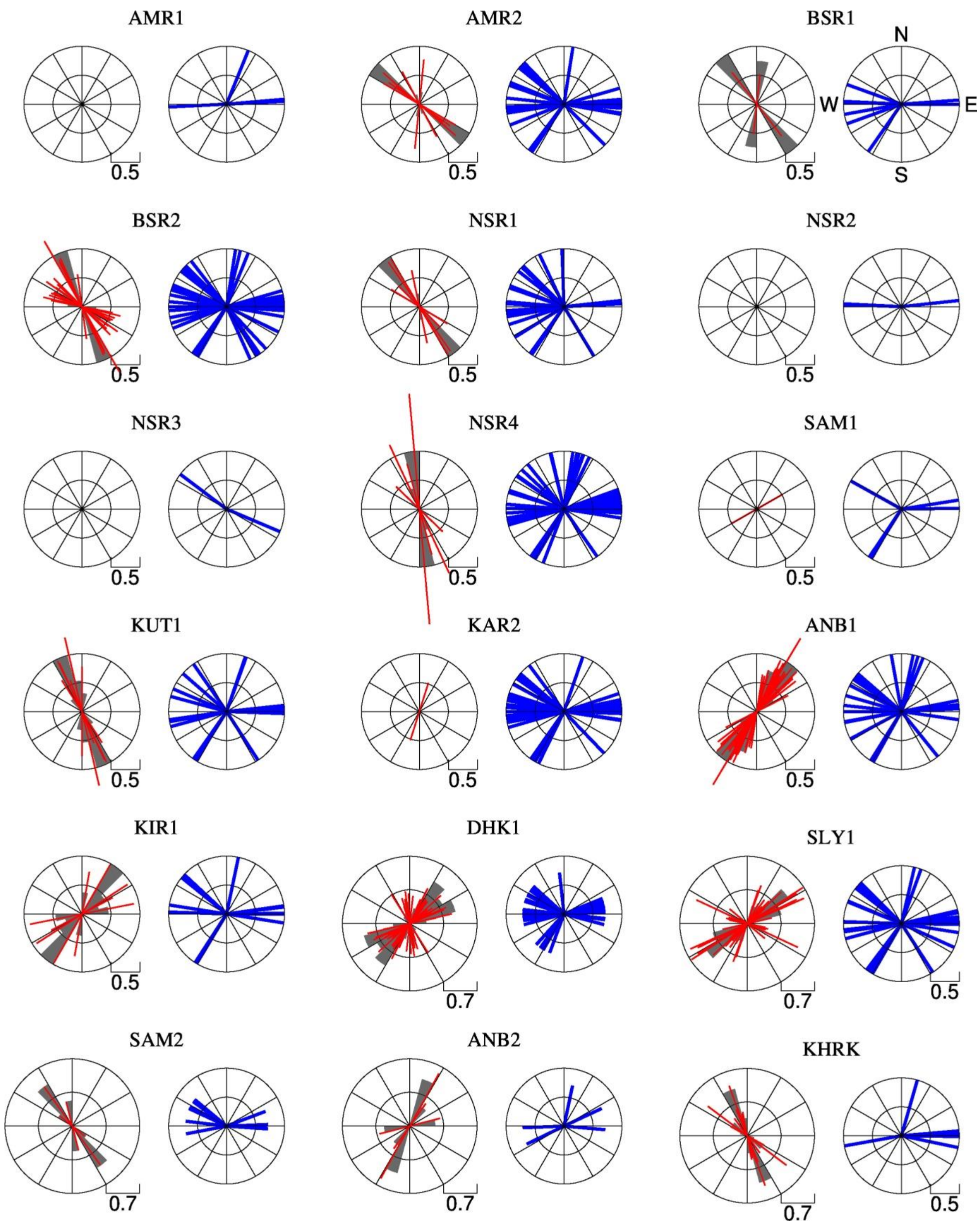

Figure 3: Rose plot of splitting measurements for stations used in this study. For each station, non-null measurements are shown on the left-hand side plot as red bars oriented in the fast direction with length proportional to the lag time. The initial polarization directions of null

https://doi.org/10.5194/egusphere-2025-1231
Preprint. Discussion started: 28 April 2025

measurements are shown as blue bars on the right-hand side plot. The locations of all stations are shown in Figure 1.

https://doi.org/10.5194/egusphere-2025-1231
Preprint. Discussion started: 28 April 2025

Figure 4

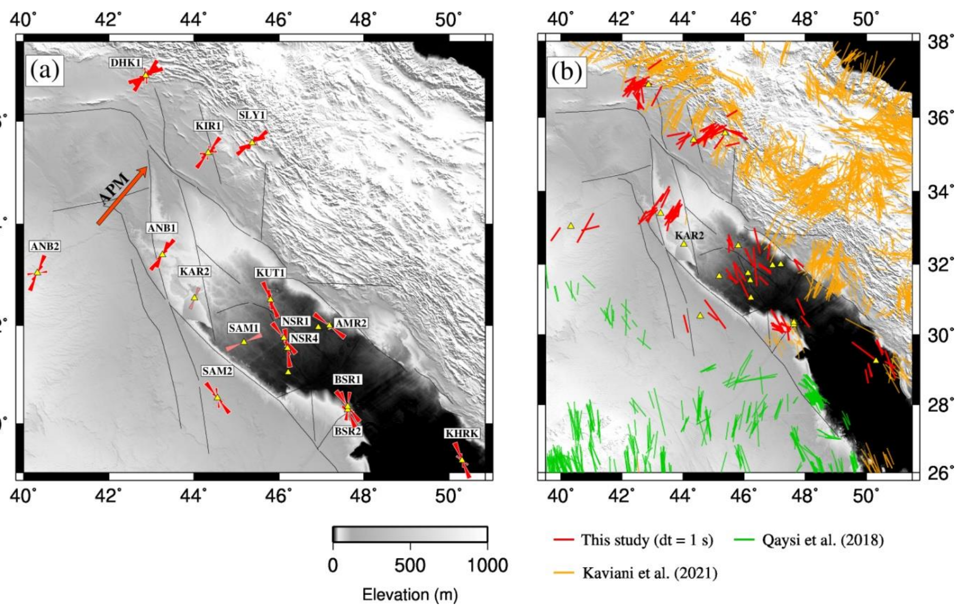

Figure 4: (a) Rose plot for non-null splitting measurements at seismic station locations (triangles). Measurements for stations SAM2 and KAR2 are shown in pink, as each has only one non-null observation. Arrow represent absolute plate motion (APM) vector from Kreemer et al. (2014). (b) Individual fast-axis orientations from this study (red bars) and previous studies by Qaysi et al. (2018) and Kaviani et al. (2021), projected onto the ray-piercing points at a depth of 200 km. Topographic and bathymetric data were obtained from the ETOPO1 global relief model (NOAA NCEI, 2022).

https://doi.org/10.5194/egusphere-2025-1231
Preprint. Discussion started: 28 April 2025

Figure 5

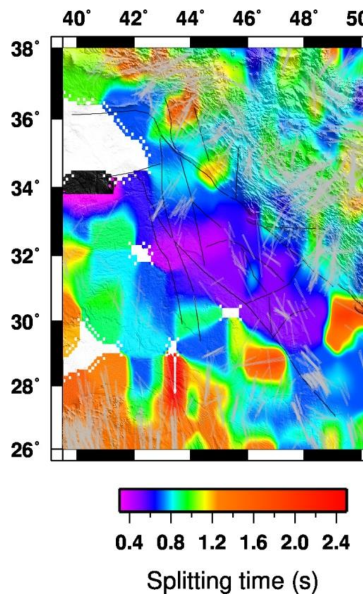

Figure 5: Distribution of spatially averaged splitting times within the Zagros Foreland and surrounding regions. Thin gray bars represent the anisotropy fast axis orientations, with their lengths scaled to match the splitting times.

https://doi.org/10.5194/egusphere-2025-1231
Preprint. Discussion started: 28 April 2025

Figure 6

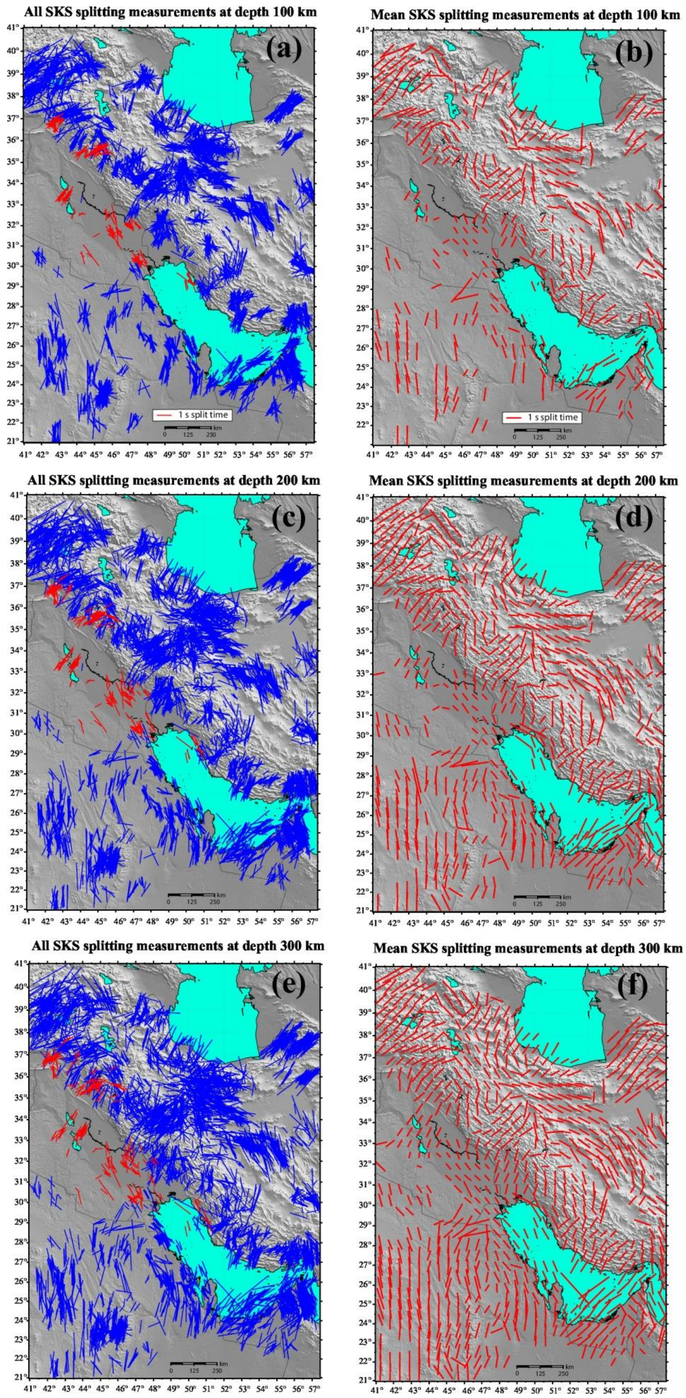

https://doi.org/10.5194/egusphere-2025-1231
Preprint. Discussion started: 28 April 2025

Figure 6: Anisotropic fast axis orientations from the current study (depicted by red bars in the left panels) combined with prior measurements (represented by blue bars) from Kaviani et al. (2021), Arvin et al. (2021), Sadeghi-Bagherabadi et al. (2018a and 2018b), and Qaysi et al. (2018). The left panels illustrate the fast axis orientations projected onto the ray-piercing point at depths of (a) 100 km, (c) 200 km, and (e) 300 km. The right panels display interpolated anisotropy fields at depths of (b) 100 km, (d) 200 km, and (f) 300 km. Elevation data were derived from ETOPO1 (NOAA NCEI, 2022).

https://doi.org/10.5194/egusphere-2025-1231
Preprint. Discussion started: 28 April 2025

Figure 7

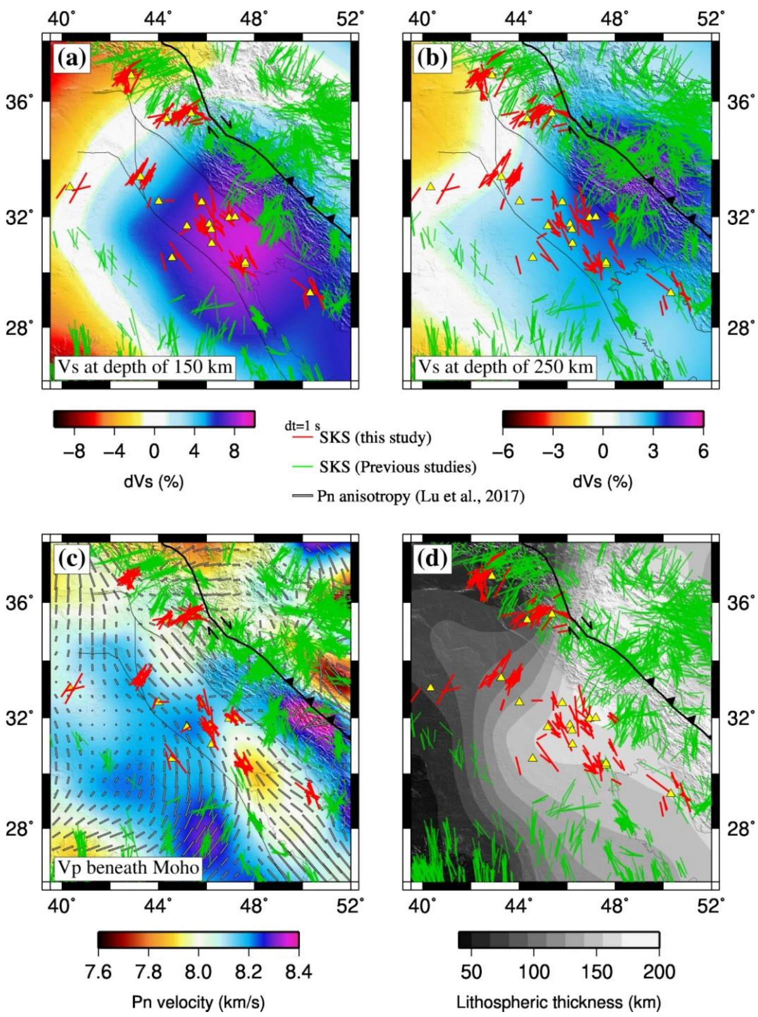

Figure 7: (a) Shear-wave velocity (Vs) map at a depth of 150 km from regional full-waveform tomography by Celli et al. (2020). Colored bars represent individual fast-axis orientations from this study and previous studies, projected onto ray-piercing points at a depth of 150 km. Thin black lines mark the borders of Mesopotamian Foredeep and Al-Jazira (Sissakian et al., 2017). (b) Same as (a), but at a depth of 250 km. (c) Pn velocity map with fast-axis anisotropy orientations (gray bars) from Lu et al. (2017), overlaid with individual fast-axis orientation measurements projected to a depth of 75 km. (d) Lithospheric thickness map from Priestley

https://doi.org/10.5194/egusphere-2025-1231
Preprint. Discussion started: 28 April 2025

and McKenzie (2013), with colored bars representing the individual fast-axis orientations projected onto ray-piercing points at a depth of 250 km. Elevation data were derived from ETOPO1 (NOAA NCEI, 2022).

Table 1. Summary of the used stations in this study and their splitting parameters. The table shows the station location, the circular mean of the fast axis orientation ($\overline{\varphi}$), the mean splitting time ($\overline{\delta t}$), the number of splitting measurements (SM), and the number of null measurements (NM). Stations with bimodal fast axis orientations are marked with an asterisk (*).

Station	**Latitude**	**Longitude**	**Begin date (YYYY/MM)**	**End date (YYYY/MM)**	$\overline{\varphi}$ **(o)**	$\overline{\delta t}$**(s)**	**SM**	**NM**
AMR1	31.9590	46.9286	2015/03	2015/10	-	-	0	8
AMR2	31.9899	47.1902	2015/11	2022/08	-42°	0.65	8	52
ANB1	33.401	43.2576	2018/10	present	32°	0.76	31	44
ANB2	33.0375	40.320	2023/06	present	42°	1.15	3	5
BSR1*	30.3581	47.6153	2014/08	2015/08	-19°	0.61	2	8
BSR2	30.2927	47.6191	2015/09	present	-43°	0.70	16	93
DHK1*	36.8606	42.8665	2014/01	present	38°	0.81	32	74
KAR2	32.5398	44.0224	2017/01	2023/02	17°	0.52	1	94
KIR1	35.388	44.3419	2018/09	2021/08	44°	0.74	7	17
KHRK	29.2543	50.3133	2021/04	present	-29°	0.86	9	7
KUT1	32.509	45.797	2021/11	2023/02	-19°	0.87	6	32
NSR1	31.7416	46.1151	2014/08	2017/09	-35°	0.69	6	40
NSR2	31.5550	46.1374	2014/07	2014/09	-	-	0	3
NSR3	31.0514	46.2199	2014/07	2014/11	-	-	0	2
NSR4	31.540	46.202	2017/10	present	-16°	1.02	5	68
SAM1	31.661	45.183	2020/12	2021/11	60°	0.51	1	6
SAM2	30.5295	44.5587	2023/03	present	-33°	1.12	3	14
SLY1	35.5784	45.3667	2015/09	present	38°	0.98	25	63